Leiden University

Minor Master Thesis

The curious case of HLX-1

Author:
Sebastiaan Haffert

Supervisors:
Prof.dr. Simon Portegies Zwart
Dr. Nathan de Vries

Computational Astrophysics
Leiden Observatory

August 2014

LEIDEN UNIVERSITY

Abstract

Faculty of Science and Mathematics
Leiden Observatory

Minor Master Thesis

The curious case of HLX-1

by Sebastiaan HAFFERT

Full hydrodynamical simulations are carried out with smoothed particle hydrodynamics to calculate the effects of tidal energy dissipation of main sequence stars that encounter intermediate mass black holes. And see if the stars can be captured through this mechanism by intermediate mass black holes. This is done to explain the curious origin of the companion star of HLX-1. The effect of tidal energy dissipation is larger by orders of magnitude than previous methods and theories predict. The tidal capture radius has been under-estimated. With the calculated capture rates of this work it would be possible to explain the origin of a companion around intermediate mass black holes in young open clusters like in the case of HLX-1 by tidal capture.

Contents

Abstract i

1 Introduction 1
1.1 HLX-1 . . . 1
1.2 AMUSE . . . 2

2 Background 3
2.1 Newton's Gravity . . . 3
2.1.1 Impact Orbits . . . 4
2.1.2 Pericenter . . . 4
2.1.3 Tidal Field . . . 6
2.1.4 Smoothed Particle Hydrodynamics . . . 6

3 Simulation Setup 7
3.1 Structure of the Code . . . 7
3.1.1 Setup State . . . 7
3.1.2 Two Body state . . . 10
3.1.3 Hydro state . . . 13

4 Results 20
4.1 Results . . . 20

5 Discussion 26
5.1 Tidal cross section . . . 26
5.2 Simulation Spikes . . . 28

6 Conclusion 29
6.1 Conclusion . . . 29

Bibliography 30

Chapter 1

Introduction

1.1 HLX-1

HLX-1[1] is suspected to be an intermediate mass black hole which emits a periodic signal. This periodic signal is of the order of 10^{41} ergs/cm^2/s in the X-ray regime. These super luminous signals are thought to originate from a companion star which transfers some of its mass to the intermediate mass black hole at pericenter[2]. One possible way to create such a system is through tidal capture[3, 4]. When a star has a close encounter with another body it will feel a gradient in the gravitational field. This gives rise to a tidal field which distorts the star when it passes the pericenter of the orbit. The distortion of the star requires energy which can only come from the orbit. If the star is initially unbound to the other body, the amount of energy it loses could be enough to make it bound. The main question is then how much energy does the star lose during its orbit due to tidal energy dissipation.

There are three approaches to solve the problem of tidal capture. One of the first theories is the linear theory [5] where the interaction is expanded in spherical harmonics. This method is a spectral method, and thus intrinsic linear, because the spherical harmonics are found to be the eigen modes which can be driven by a stellar encounter[6]. The resulting decomposition leads to adiabatic non-radial oscillations in the star. It is found that the most dominant oscillations are the $l = 2, m = 0$ and the $l = 2, m = \pm 2$ modes[6, 7]. These two mode represent a rotation of the star perpendicular to the orbital plane and a travelling wave of higher frequency.

A second method describes [8, 9] the deformation of the star as it encounters a massive point particle in non- and relativistic settings. The gradient in the gravitational field causes a slight deformation of the star. Deformations are easiest described in the

Lagrangian form where the effect of an external potential on a small fluid element is considered. In this formalism internal energy generation can also be accounted for. The total interaction can be described as a deformation tensor in the case of linear deformations of the star. This results in a tensor equation for the semi-major axes of the star during the orbit. The described expansion or compression of the star needs energy which comes from the orbit of the star. An analogous model for incompressible fluids was created in the early '70 [10]. The method of linear deformation was improved by [11, 12] which include non-linear effects making it possible to calculate the effect of large tidal fields on stars. The non linear effects cause a higher energy deposition of into the star when passing the pericenter than the linear models predicts. It is thus likely that tidal effects have been underestimated if only the linear models is considered.

The third approach is doing the full hydrodynamical calculations to calculate the dissipated energy. Several [13–16] 3d hydrodynamical simlations have been done to try to measure the effects of tidal forces. Both grid based methods and smoothed particle hydrodynamics based methods have been done. A problematic factor is the fact that almost al simulations done have very different setups. These range from different kind of polytropic models used for the stars to the type of perturber that is used to excite the star. This limits how well they can be compared with each other. One thing in which all simulations agree is that the energy loss is higher than predicted by the linear model of [5]. But until now most simulations have focused on close encounters, close to the tidal disruption limit. This is mostly due to the limit of precision of the energy conservation, since energy dissipation by tidal interaction is a small effect. In this thesis the parameter space of weak encounters is explored to find the outer limits of tidal capture.

1.2 AMUSE

AMUSE[17], which is short for Astrophysical Multipurpose Software Environment, is a software package written in Python for astronomical simulations. It is an intermediator between several highly optimised simulation codes which are written in different programming languages. AMUSE can be used to simulate physics on different scales by combining several of these optimised codes making it a good choice for simulating tidal captures.

Chapter 2

Background

2.1 Newton's Gravity

The orbits of celestial bodies can be calculated, to high accuracy, with Newton's law of Gravity. If there is a system consisting of N particles the force of particle i on particle j is then given by

$$\vec{F}_{ij} = -G\frac{m_i m_j}{r_{ij}^2}\hat{r}_{ij} \tag{2.1}$$

Where m_i and m_j are the masses of the bodies, r_{ij} the distance between the particle i and j and G the universal gravitational constant. $\hat{r}_{12}$ is the direction from particle i to particle j. These systems are called N body systems and a general solution for a system with $N \geq 3$ is not possible. When the total system exists of 2 particles it has an analytical solution, the Kepler orbit which is

$$r(\theta) = \frac{a\left(1-\epsilon^2\right)}{1+\epsilon\cos\left(\theta-\theta_0\right)} \tag{2.2}$$

where r is the separation distance between the two bodies, a is the semi-major axis, ϵ is the eccentricity of the orbit, θ is the angle the orbit makes with semi-major axis and θ_0 describes the initial phase. A Kepler orbits can geometrically be described as conic sections. The eccentricity ϵ determines the kind of conic section. Elliptical and circular orbit with eccentricities of $0 \leq \epsilon < 1$ are bound orbits, parabolic and hyperbolic orbits are unbound and have eccentricities of $1 \leq \epsilon < \infty$. A parabolic orbit has an energy of precisely zero and an eccentricity of 1. In this work near parabolic orbits are used since these have a slightly positive total energy and thus have the highest chance of being captured due to tidal interactions.

2.1.1 Impact Orbits

A successful tidal capture happens when an unbound orbit changes to a bound orbit due to tidal interactions. Unbound orbits can always be described as orbits coming from infinity. This follows quite easily from energy conservation. The energy for a Kepler orbit is

$$E = \frac{1}{2}mv_1^2 + \frac{1}{2}Mv_2^2 - G\frac{Mm}{r} \tag{2.3}$$

where m is the mass of the body that is shot with a speed of v_1 towards the heavier object with mass M with a speed of v_2 and r is the distance between the two bodies. If the orbit starts at infinity the energy will always be $E \geq 0$, which is the condition for an unbound orbit. These orbits can be parametrised with 2 parameters, the initial relative velocity v_∞ of the particle that is being shot and an impact parameter b. The impact parameter is the perpendicular distance between the two bodies at infinity. There is no loss of generality when using these two parameters if the particle from infinity has a velocity which is not oriented towards the other body. In that case the whole coordinate system can be rotated. So all possible impact orbits can be made by using the two parameters b and v_∞. For tidal captures the star is shot from infinity towards the black hole.

FIGURE 2.1: An impact orbit. The smaller sphere is the particle that comes from infinity and the larger sphere is the body that is being shot. The impact parameter b is the distance between the centers of the spheres. The initial momentum p is the momentum of the star in infinity.

2.1.2 Pericenter

The pericenter is defined as the point of closest approach between two objects. This is an important point from the view of tidal dissipation since it determines the tidal interaction strength. The closer the star approaches the black hole the higher the energy loss will

be. The pericenter distance for an impact orbit is given[18] by

$$r_{min} = \sqrt{\frac{G^2 M_{bh}^2}{v_\infty^4} + b^2} - \frac{GM_{bh}}{v_\infty^2} \tag{2.4}$$

This will also be used to validate the starting point of the simulation in subsection 3.1.2. From this equation the impact parameter can also be determined if the pericenter distance is known.

$$r_{min} = \sqrt{\frac{G^2 M_{bh}^2}{v_\infty^4} + b^2} - \frac{GM_{bh}}{v_\infty^2} \tag{2.5}$$

$$r_{min} + \frac{GM_{bh}}{v_\infty^2} = \sqrt{\frac{G^2 M_{bh}^2}{v_\infty^4} + b^2} \tag{2.6}$$

$$b^2 = \left(r_{min} + \frac{GM_{bh}}{v_\infty^2}\right)^2 - \frac{G^2 M_{bh}^2}{v_\infty^4} \tag{2.7}$$

$$b^2 = r_{min}^2 + 2\frac{GM_{bh}}{v_\infty^2} r_{min} \tag{2.8}$$

This can be used to calculated the cross section for different collision processes. For a direct collision without gravitational interaction the minimal distance needed for a collision is $r_{rmin} \leq R + R_{bh}$. The corresponding cross-section is then

$$\sigma = \pi(R + R_{bh})^2 \tag{2.9}$$

If the particles interact by gravity the cross section becomes larger due to gravitational focussing. The cross section for a collision with gravitational focussing is given by

$$\sigma = \pi(R + R_{bh})^2 + 2\frac{GM_{bh}}{v_\infty^2}(R + R_{bh}) \tag{2.10}$$

This can be recognised as equation 2.8 with $r_{min} = R + R_{bh}$. A related parameter that is the dimensionless tidal interaction parameter which is defined as

$$\eta = \left(\frac{M_{star}}{M_{star} + M_{bh}}\right)^{\frac{1}{2}} \left(\frac{r_{min}}{R}\right)^{\frac{3}{2}} \tag{2.11}$$

The energy loss due to tidal interactions is a function of η. When this function has been found by using simulations it can be inverted to find η as function of the energy loss. Then the above equation can be used to find the corresponding r_{min} and that can be used to find the cross section of tidal interactions.

2.1.3 Tidal Field

When an object has a certain extent the amount of gravity the object feels throughout its own body changes with position. This can be described by a tidal field in first order approximation. Suppose that a star with a radius of R is orbiting a heavier black hole such that $M_{bh} \gg M_{star}$. The movement of the black hole can than be neglected. The amount of gravity the star feels at the points closest and farthest from the black hole can be expressed as

$$F = -G\frac{M_{bh}M_{star}}{(r \pm R)^2} = -G\frac{M_{bh}M_{star}}{r^2}\frac{1}{\left(1 \pm \frac{R}{r}\right)^2} \tag{2.12}$$

The plus or minus determines whether the back or the front of the star is considered. When the star is orbiting far away from the black hole such that $r \gg R$ a Taylor expansion can be made of the second term on the rightmost equation.

$$F = -G\frac{M_{bh}M_{star}}{r^2} \pm G\frac{2M_{bh}M_{star}}{r^2}\frac{R}{r} + \mathcal{O}\left(\left(\frac{R}{r}\right)^2\right) \tag{2.13}$$

The difference between the front and backside of the star is the tidal force.

$$F_{tides} = G\frac{4M_{bh}M_{star}R}{r^3} + \mathcal{O}\left(\left(\frac{R}{r}\right)^2\right) \tag{2.14}$$

It is clear that a tidal force will only exists if the star has a finite non-zero extent, which is not the case for a point particle. So a tidal interaction can't be simulated using only point particles, more advanced models of the star are necessary. The tidal force can be compared to the force on the centre of the star.

$$\frac{F_{tides}}{F} = -\frac{4R}{r} + \mathcal{O}\left(\left(\frac{R}{r}\right)^2\right) \tag{2.15}$$

2.1.4 Smoothed Particle Hydrodynamics

To simulate a star on a near parabolic orbit it is easier to work with a hydrodynamical method which does not depend on a grid so that the geometry can change freely. This can be done with the smoothed particle hydrodynamics method (SPH) introduced by Gingold and Monaghan [19]. In SPH a fluid or gas is modelled by particles which interact with each other. To get a hydrodynamical quantity the particles are convolved by a kernel to estimate it. This can then be used to solve the equations of motion for the fluid. An overview of the SPH technique and recent developments can be found in a review by Rosswog [20].

Chapter 3

Simulation Setup

3.1 Structure of the Code

The tidal capture simulation consists of four states. Every state handles a different part of the simulation. The breakup in several states was done to handle the multi scale aspect of the problem at hand. For each scale a different state is made where the physics are solved appropriately. Tidal dissipation is a problem on 2 scales; the star and the black hole are simulated as point particles when the distance is large, and the system is treated with full hydrodynamics if the distance is small. The general overview of the simulation can be seen in the flow diagram in Figure 3.1.

3.1.1 Setup State

The set-up state prepares everything that is necessary for the simulation. The most important part during this process is the creation of a good SPH star model. First the stellar evolution code EvTwin [[21], [22]] is used to create a realistic density profile for a star with $M_* = 1.0\ M_\odot$ and solar like metallicity. The star is evolved to an age of 1 Myr. Further evolution of the star is not necessary since the radius of the star barely changes during the main sequence. In Figure 3.2 the change of the radius is plotted against time. In the method described by Press and Teukolsky [5] the amount of energy that is being dissipated in a stellar encounter is dependent on the radius of the star. For the considered star the radius only increases by about 2 percent in 1 Gyr, which is negligible. The age of the star is therefore not relevant for the tidal simulation. So to save some computing time the star is evolved to an age of 1 Myr.

The star model is converted to a SPH model by distributing the particles in a grid in such a way that the density profile matches the star model from the stellar evolution

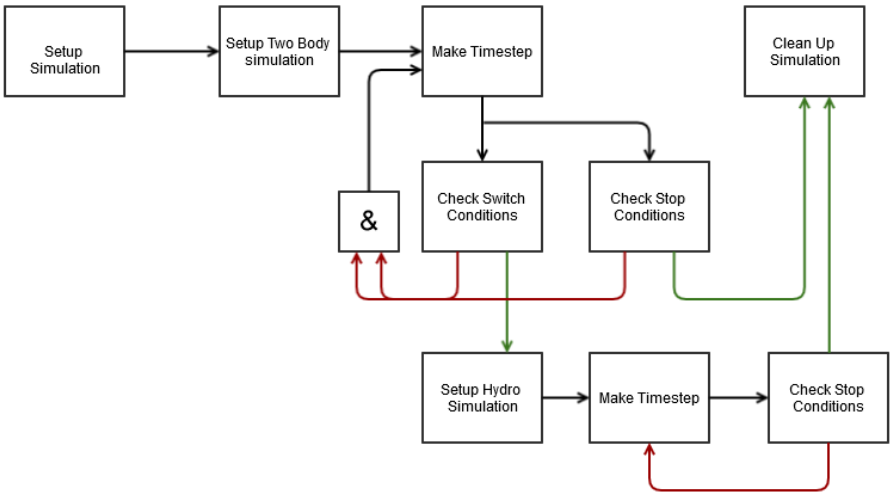

FIGURE 3.1: Flow chart of the simulation. The four states of the simulation are the set-up state where all preparation for the simulation takes place. The two body state which simulates the system on the largest scale as a Kepler orbit. The hydro state where full 3D hydrodynamical interactions are calculated and the clean up state where the whole simulation is nicely wrapped up. If a condition is met the output line is green and if the condition is not met the output line is red. Black lines are flow lines of the program when it is not possible to branch.

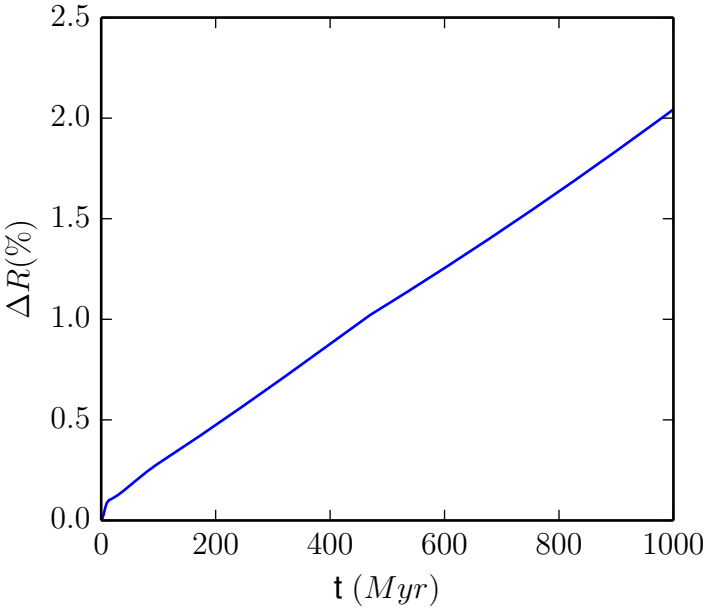

FIGURE 3.2: The change of radius in percentage against time for a 1 $M_{\odot}$ mass star with solar metallicity.

code. The grid can be chosen in a few different ways. A several types of regular grids or a random grid. The random grid sampling was chosen to reduce possible artefacts due to an artificial structure in the sampling of the density. The conversion of stellar model to SPH model is not perfect. The amount of particles used to replicate the structure the star all have equal mass and that limits the mass resolution. This means that the density profile can't be well replicated in the outer edge of the star where the density is low. So the actual radius of the simulated star is smaller than the actual radius given by the stellar evolution code. The amount of particles that is used is 5000. With a particle resolution of $N = 5000$ the mass resolution is $M_i = 0.0002 M_\odot$. Density structures that are smaller than this mass resolution can not be reproduced. The actual radius of the star thus depends strongly on the amount of particles that is used.

Another artefact from generation with a finite number of particles is that the SPH clouds that are created are not in hydrostatic equilibrium. So each time a SPH star is made from a stellar model it needs to be relaxed, otherwise it will oscillate during the simulation. This relaxation is done with a target velocity, so that after the relaxation the star has the target velocity as center of mass velocity. To achieve control over the center of mass velocity a simple proportional feedback controller is used. For proportional feedback the deviation from the target velocity is calculated and then subtracted with a gain factor from the velocity of the particles. The gain factor should be smaller than 1 otherwise the system will explode. Using the feedback relaxation any center of mass velocity can be reached. An example of a relaxation with a target velocity of zero can be seen in Figure 3.3. The energy in the center of mass velocity is reduced by 2 orders of magnitude and the internal energy also slowly changes. What is clear from the Figure is that while the center of mass kinetic energy is low the internal energy hasn't converged yet. So after a dampened evolution the star is also evolved without any constrains.

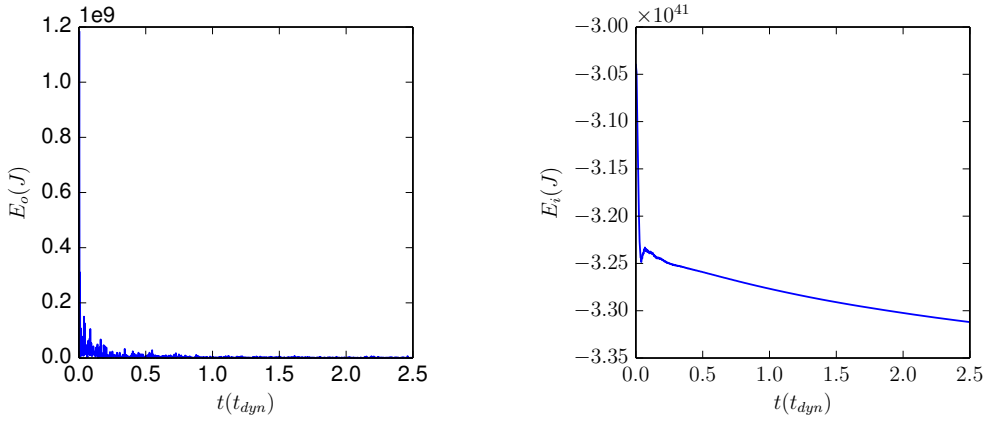

FIGURE 3.3: The dampened evolution of the kinetic energy (left) and the internal energy (right).

Since the star is not in a steady state the semi-axes of the ellipsoid will also change considerably. The semi-axes are calculated by using the principle axes of the moment of inertia tensor. The position of the particles are projected on each eigen vector of the inertia tensor. After which the 10 largest projections are averaged to get the semi-axis in that direction. During the dampening of the star the semi-axes of the star change considerable as can be seen in Figure 3.4. It is thus important to account for the change of radius when comparing the simulation with the analytical methods.

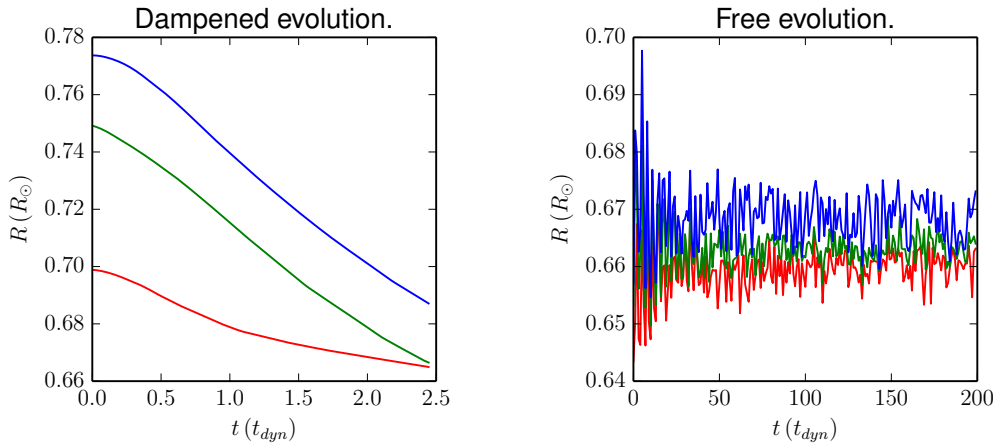

FIGURE 3.4: The evolution of the semi-axes during the dampened relaxation of the SPH cloud. The initial values of the semi-axes are very different. During the evolution the axes change considerably.

The effect of the dampened evolution on the semi-axes of the star can be seen in Figure 3.4. During the dampened evolution the semi-axes do not converge. To let the star converge it is also evolved without any constrain. In Figure 3.4 the plot on the right is the evolution without dampening. During this stage the semi-axes converge after about 50 time steps.

3.1.2 Two Body state

In the two body state the star and the black hole are simulated as point particles. The particles are evolved in time by using a semi-analytical method to solve the Kepler orbit. After each time step the orbit is checked for state change conditions. There are two state change conditions in the two body state. The first is a switch condition which determines when to go to the full hydrodynamical treatment. This conditions is based on the relative force on the edges of the star compared to the central force as in equation 2.15. When this force exceeds a certain percentage F the code is switched from a two body problem to the full hydrodynamical treatment. F is named the threshold value

in this work. The tidal force calculation can be converted in a distance conditions by manipulating equation 2.15.

$$F \leq |-\frac{4R}{r}| \tag{3.1}$$

$$F \leq \frac{4R}{r} \tag{3.2}$$

$$r \leq \frac{4R}{F} \tag{3.3}$$

The state is switched from the two body problem to a full hydrodynamical problem when the distance is smaller than $\frac{4R}{F}$. A low value of F means the hydrodynamical treatment starts far away from the black hole and for a high value of F it starts closer to the black hole. The threshold value also determines when the simulations are stopped. When the star reaches the threshold again after passing the black hole the simulation will be stopped. Thus the threshold value determines how long the computation of a single simulation is going to take.

Another point of consideration is that when the threshold value is too high it can happen that the important part of the orbit, where the tidal interaction is dominant, is neglected. So to determine when to switch from the two body model to the hydrodynamical model it is necessary to know for which F the simulations converge in the amount of energy that is lost during the pericenter passage. The amount of energy that is being lost is the difference between the orbital energy at the initial threshold and the orbital energy at the final threshold. The SPH star is used for this calculation and the orbital energy is defined as

$$E_o = \frac{1}{2}M|\vec{v}_{cm}|^2 - \sum_{i=1}^{i=N} G\frac{m_i M_{bh}}{r_i}, \tag{3.4}$$

where the index of summation is over all particles bound to the star, M is the total mass of particles bound to the star and $\vec{v}_{cm}$ is the center of mass velocity of all the bound particles. r_i is the distance from a particle to the black hole. The determination when a particle is bound is explained in section 3.1.3.

The results of five runs with the same initial conditions but with varying threshold value are plotted in Figure 3.5. The threshold value that is chosen for all further simulations is $F = 0.005$, since for that value the signal to noise ratio is highest.

The second state change condition is a stopping condition. When the star is past the pericenter of it's orbit but the distance to the black hole is beyond the threshold distance the simulation will be stopped.

One thing to keep in mind is that the orbits need to be impact orbits which are defined as coming from infinity. A good sanity check is to see whether or not the distance from

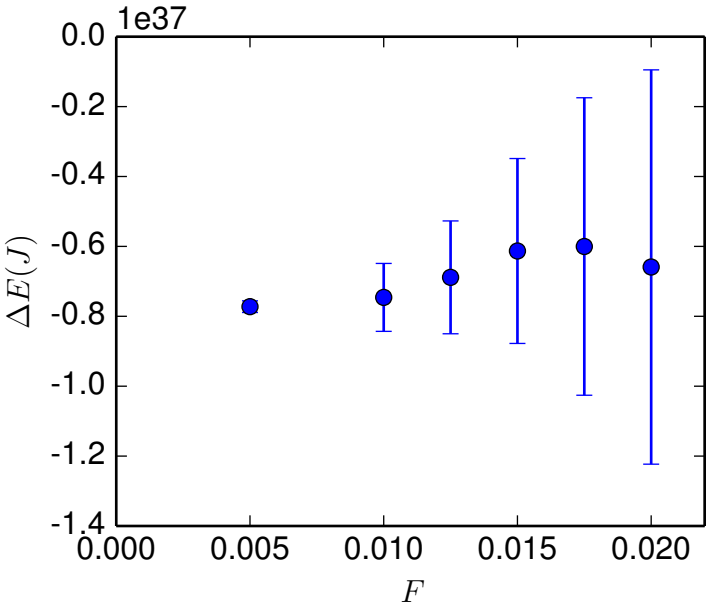

FIGURE 3.5: The energy loss during a nearly parabolic orbit against different threshold values. The energy loss converges at a F value of 0.005.

which the two body simulation starts is far away enough so that the difference between this orbit and an orbit from infinity are negligible. Since the tidal energy dissipation is strongly dependent on the pericenter distance via η a good check is to look at the difference between the analytical pericenter distance and numerical pericenter distance. All orbits start at a distance of 10000 AU. The pericenter distance is determined by using the 10 points for which the 2 bodies were closest to each other and then fitting a parabola through the points. From Figure 3.6 can be read that the relative error with an

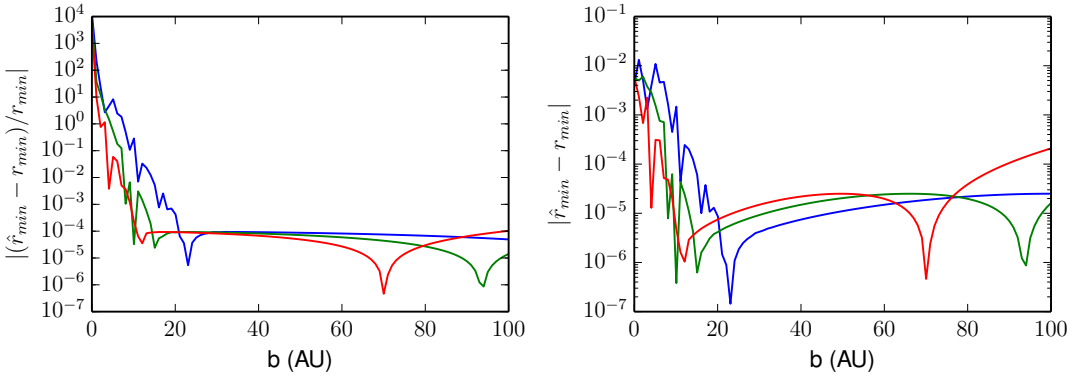

FIGURE 3.6: The pericenter as function of different impact parameters. Each line represent a different initial velocity. The orbits of the blue line have the lowest initial velocity of 30 km/s. The green orbits start with an initial velocity of 45 km/s and red has the highest of 60 km/s.

initial distance of 10000 AU is about 10^{-4}. Only when the impact parameter decreases to near 0 does the error increase. If the impact parameter is very small relative to the starting distance the eccentricity will also become very high. These orbits come very close near the black hole which means that the forces become very large. This causes integration errors and thus results in error in pericenter distance. From the Figure it is clear that the orbits are accurate from $b \geq 10$ AU.

3.1.3 Hydro state

In the hydro state the star is simulated using full hydrodynamics. In AMUSE there are two SPH hydro codes implemented; Gadget-2 [23] and Fi[24]. Both codes are based on the SPH method and implement a tree code scheme for the gravity. During test runs it appeared that both methods are quite competitive in energy conservation, which is the most important point for these tidal captures. The main difference between Gadget and Fi is the computational time for a single simulation. Fi is on average a few times slower than Gadget the exact reason why is not clear. Gadget was chosen over Fi for the simulations since relatively many simulation have to be done.

During the simulations the energy has to be conserved to a very high degree since the effects of tidal dissipation are small. To achieve the required energy conservation several steps have to be done. The first is to relax the star as was described in section 3.1. The star that is made during the relaxation is stored on the disk so that it does not have to be relaxed every time a new simulation is started. A very surprising effect is that every time Gadget is loaded with a new SPH particle set it needs to be relaxed again, even if that particle set is a relaxed particle set. In Figure 3.7 the star is evolved for about 300 dynamical timesteps after which the star is stored to the disk. Then the star is reloaded and evolved again for about 50 dynamical timesteps.

Around the 300th timestep a large jump appears and that is exactly when the particle set is reloaded. The jump also causes the star to converge to a different internal energy state. If the star would be just loaded from the disk it would be difficult to measure an energy loss since the beginning would be highly dynamic due to the relaxation process. So each time a particle set is loaded it needs to be relaxed again. This is named the 'burn in' of Gadget throughout this work. The cause of this jump is probably due to non initialized internal variables of Gadget, but this needs further investigation to fully know where the effect comes from. After the burn in of gadget the star should be fully relaxed.

During the test runs it became clear that a tree code would not be accurate enough to get the required energy conservation. An example of the bad energy conservation

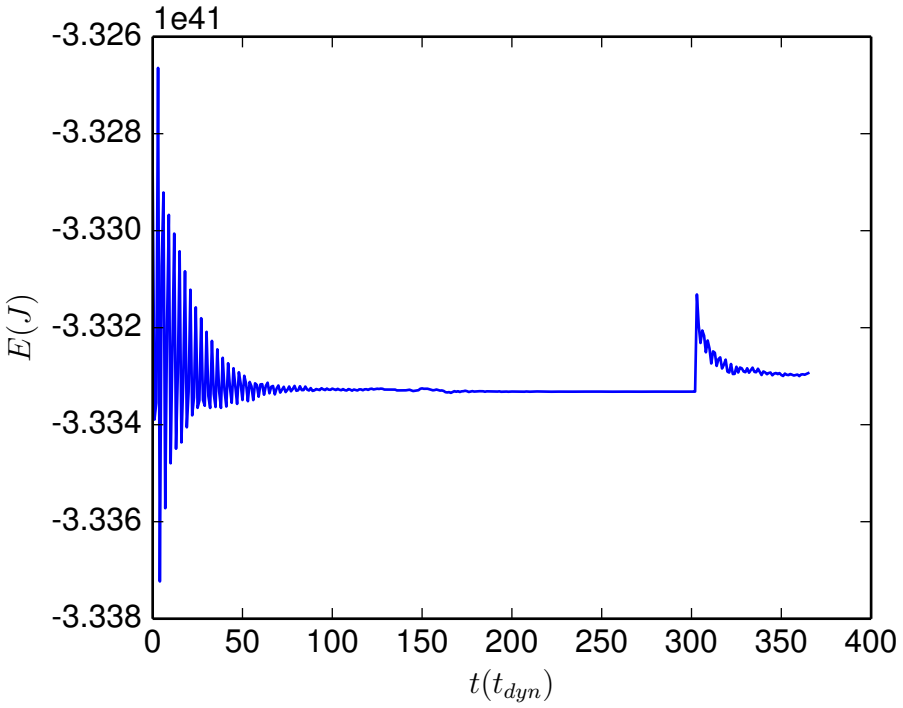

FIGURE 3.7: The energy evolution during a constrain free simulation. The energy oscillates heavily until about 100 dynamical time steps. After 300 times step the particle set is written to the disk. Then the same particle set is reloaded and evolved further for another 75 time steps. A clear jump in energy can be seen at the reloading point. The SPH cloud converges to a different energy state with the reloaded particle set.

can be seen in Figure 3.8. To increase the accuracy of a tree code the opening angle can be decreased. In a tree code multipole moments are calculated to approximate the gravitational force. So a single particle that looks at particles far away will see a single clump. The opening angle represents the normalised solid angle of the clump and if that opening angle is larger than the threshold value it will break up the clump in smaller clumps. This will continue until all clumps have a opening angle smaller than the threshold value. So the force calculation can achieve higher accuracy by decreasing the opening angle. In the limit of the opening angle threshold going to zero the tree code will approach a direct sum method. This is done to acquire the required level of energy conservation. The opening angle is set to 10^{-6} in the simulations, this number was chosen arbitrarily. This effectively makes the tree code in Gadget a very slow direct sum method.

The careful relaxation and small opening are tested by doing a simulation without a black hole to see if Gadget conserves the energy to high enough precision with all the built in relaxations. The relative energy error is plotted in Figure 3.9. Using the two

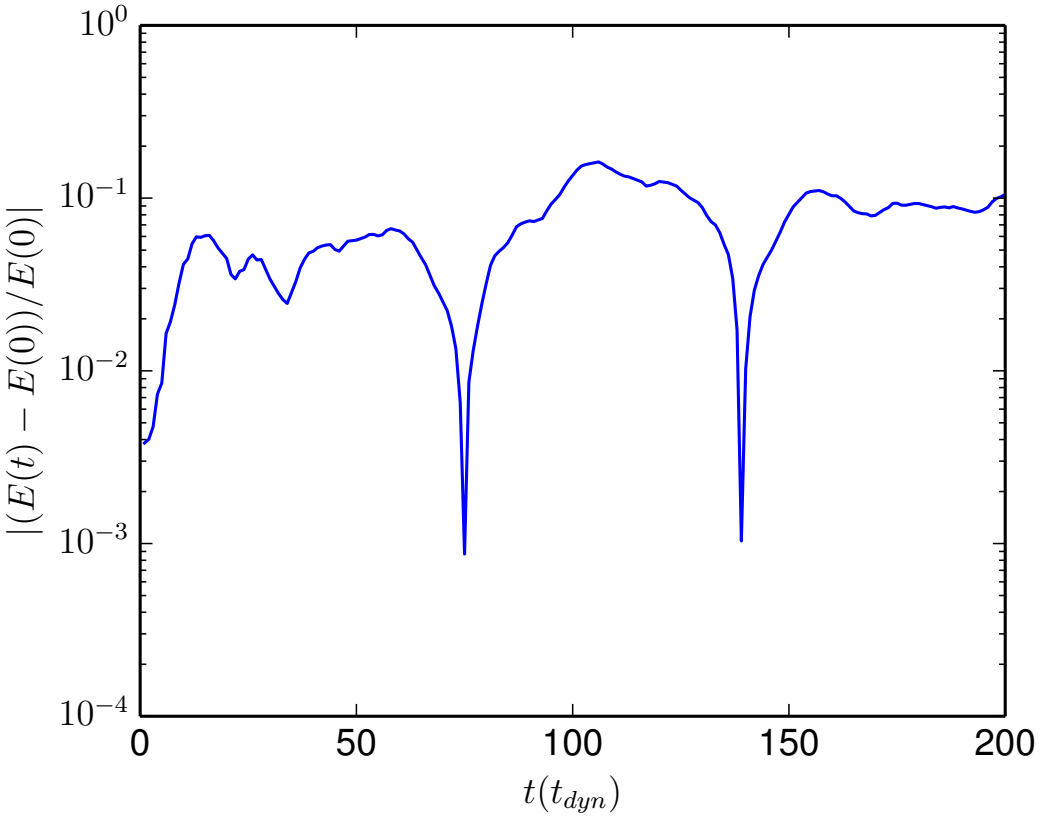

FIGURE 3.8: The energy evolution of the SPH star orbiting on a circular orbit of 50 AU around the black hole. The simulation is done with only Gadget. The energy is conserved within 10 percent.

described types of relaxation Gadget conserves the energy to about 1 part in 300000. This is precise enough to measure tidal dissipations.

The next step is to include the black hole. A second part that needs to be considered is the interaction between the star and the black hole. In Gadget gravity is calculated with a tree code which is not as accurate as a direct sum code. To improve the accuracy the interaction force between the black hole and the star is calculated by using a bridge. A bridge is a method in AMUSE to couple different codes together. The coupling between particle sets of different code is done by using kicks. During the kick the effect of two separate system on each other is calculated and applied as a momentum kick. After that the codes evolve separately which is the drift and finally it concludes with another kick. This is effectively a second order sympletic integrator. With these bridges it is possible to use a direct sum code as interaction code between the star and blackhole. To determine which code would be best as an interaction code the energy conservation of several codes was tested by simulating a close encounter with 2 particles. The same initial conditions are used for every run with $b = 100$ AU and $v_{initial} = 50$ km/s. The

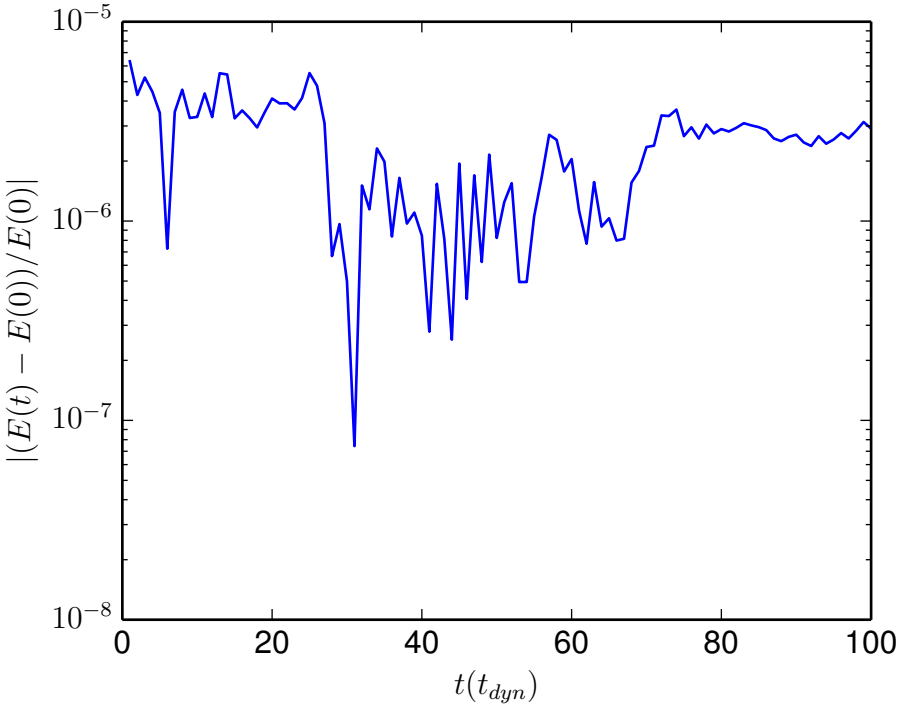

FIGURE 3.9: The energy conservation during a free evolution. The energy is conserved to about 1 part in 300000.

results are plotted in Figure 3.10. From left to right and top to bottom the codes used are Gadget, phigrape, Huayno[25] and Hermite[26]. These code were chosen because they are CPU based direct sum codes which are available in AMUSE. The code that performs the best is Hermite, but it can not be used for this problem. Hermite uses adaptive timesteps which are based on collision times for pairs of particles. At least 2 particles have to be available for Hermite to run. In the case of the tidal capture simulation only the blackhole is simulated with the interaction code so there is only one particle. Hermite falls off as a choice and the next best is PhiGrape, but while Phigrape is based on a different integrator the timestep determination is also based on pairs of particles. So the choice for an integrator fell on Huayno.

Coupling with the bridge adds another variable which influences the energy conservation. This is the bridge time step, which can be seen as how often the codes interact with each other. If the time step is too large the energy can begin to drift. In Figure 3.11 this effect can be clearly seen. In this run a circular orbit is simulated with a semi-major axis of 1 AU. The time step here is taken as $\Delta t = t_{dyn}$. The energy diverges after about 10 time steps. To solve this problem the time step has to be decreased. For Figure 3.12 the time step was taken as $\Delta t = 0.01\ t_{dyn}$. The interaction is now precise enough to be usable for measuring tidal energy dissipation.The energy conservation is better than in

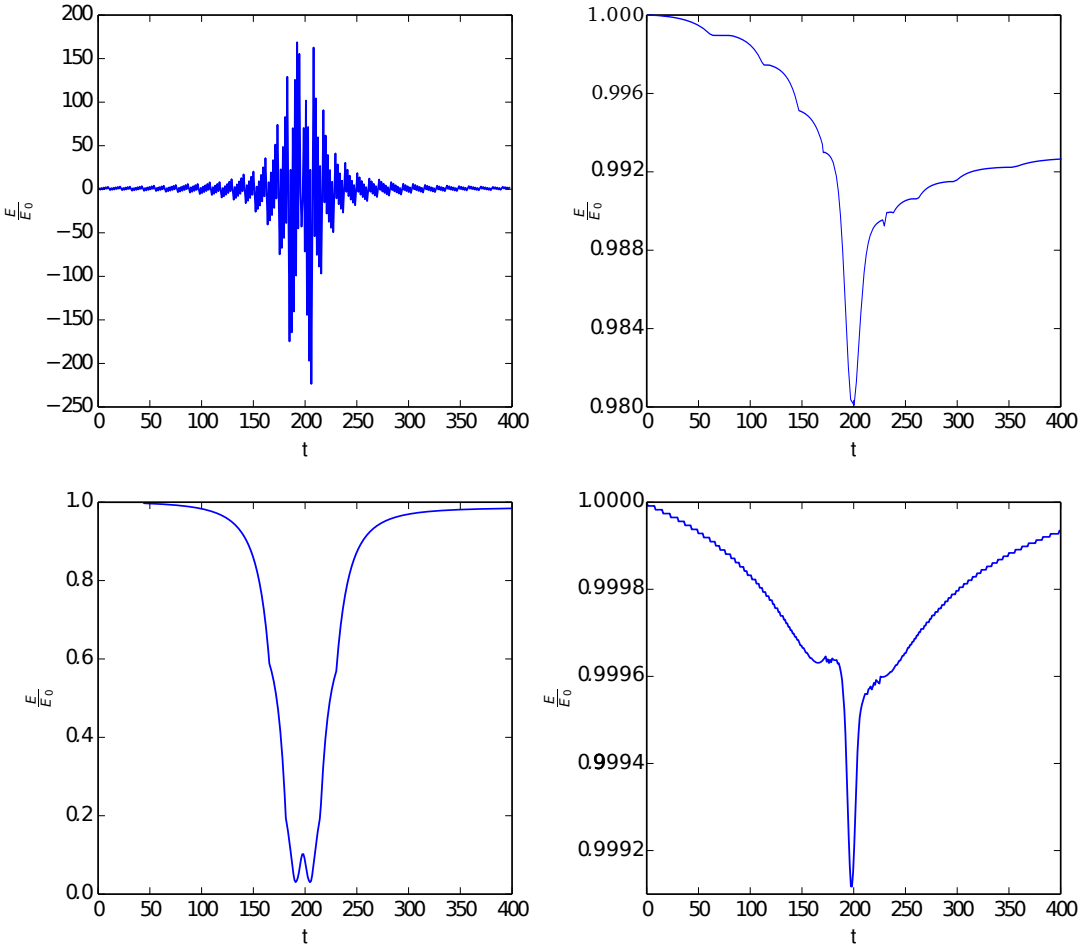

FIGURE 3.10: The energy conservation of a 2 body orbit with different integrators. From left to right and top to bottom the used integrators are; Gadget, phigrap, Huayno and Hermite. All orbits started with the same initial conditions and timestep size. Hermite has the best energy conservation and Gadget the worst.

Figure 3.9 where only Gadget is used to evolve the SPH particles. This is because the time step is taken smaller. To be absolutely sure the energy stays conserved during the tidal dissipation runs the timestep has been set to $\Delta t = 0.005\ t_{dyn}$. With this timestep choice a single run takes between 6 - 6.5 hours.

After each timestep the bound particles of the star are determined. First the center of mass is calculated of all particles. This center of mass will be not the true center of mass of the bound particles because if there are unbound particles they can shift the position by quite a lot. So the center of mass determination of the bound particles is done in 2 steps. After the first iteration the particles within 1 $R_{\odot}$ of the center of mass are selected and for those particles the center of mass is determined again. To determine if the SPH particles are bound to each other it is necessary to start with a core. The core is taken as all the particles that fall within a radius 0.1 $R_{\odot 1}$ relative to the center

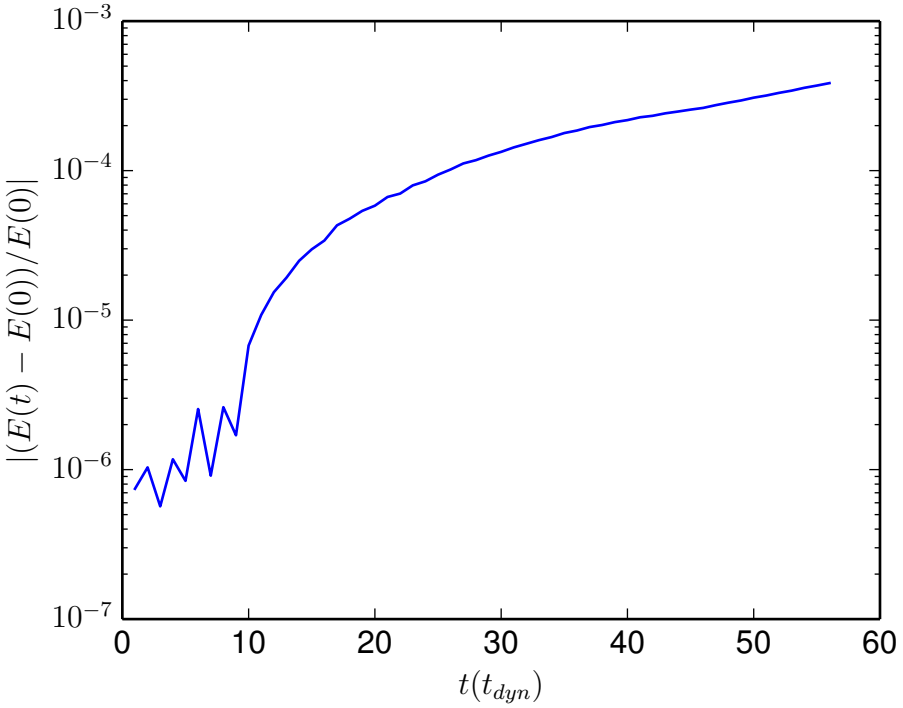

FIGURE 3.11: The energy conservation of the star on a circular orbit. The timestep of the bridge is $\Delta t = t_{dyn}$. After 10 iterations the energy diverges.

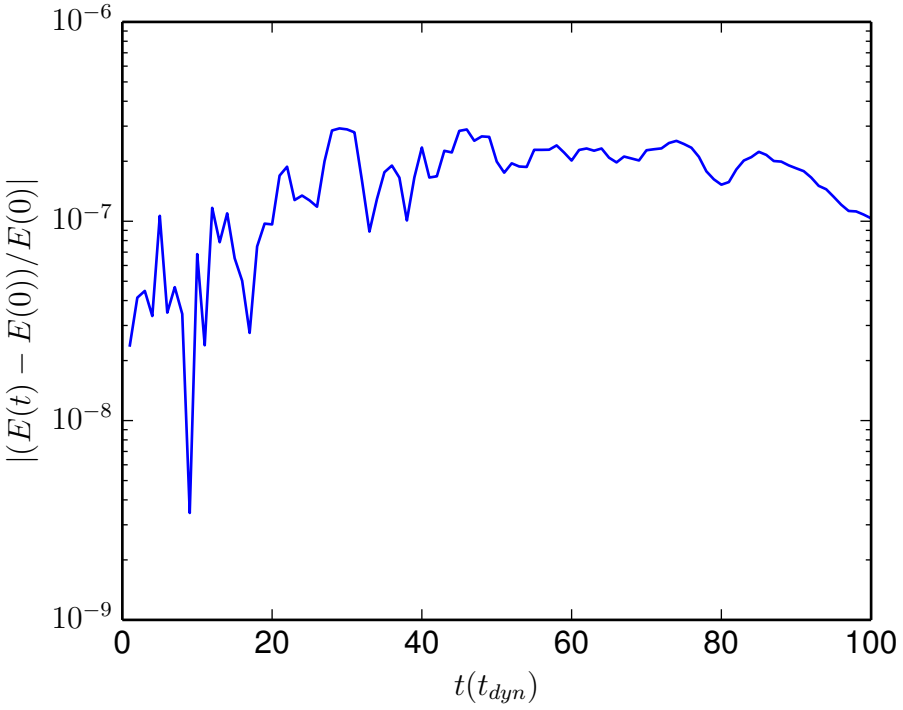

FIGURE 3.12: The energy conservation of the star on a circular orbit. The timestep of the bridge is $\Delta t = 0.01 t_{dyn}$. The relative energy error is almost 10^-7 on average.

of mass. After the core determination the bound particles have to be found. A particle is bound if the specific energy of the particle is negative. The specific energy of one particle is

$$E_i = \frac{1}{2}v_i^2 + u_i - GM_{core}/r_i \tag{3.5}$$

where v_i is the velocity of particle i, u_i is the thermal energy density, M_{core} is the mass of the core and r_i is the distance from particle i to the center of mass of the core. Every particle that has a negative energy will become part of the core. This selection algorithm will continue until no new particles are added to the core or if all particles are selected.

Chapter 4

Results

4.1 Results

The amount of energy lost is only dependent on η and η is a function of b and v_∞. So there are is an infinite number of orbits possible for each η. This makes it possible to do multiple simulation with different initial conditions but the same η. And since the energy loss only depends on η all simulations should give the same answer. The runs use 5000 particles for the SPH. These simulations lose their memory very vast so the error on each simulation should be identically independent distributed. So averaging multiple simulations would make the final result more accurate. For each η 5 different simulations are used. The initial conditions were chosen with a fixed η while varying v_∞ and using equation 2.8 and equation 2.11 to calculate the corresponding b. To find tidal captures it is important for orbits to have an eccentricity very close to 1. The closer to 1 the more likely it is that the orbit will become bound. The initial speed of the first simulation is chosen as the escape velocity on the starting point. This would make the total energy of the orbit close to zero. For the other 4 simulations the initial speed is increased in steps of 5 % with respect to the first speed. The energy loss for the linear model are calculated with the fit made by [27].

From Figure 4.1 can be seen that like all the previous simulation the energy loss is more than the linear model predicted. In the strong coupling regime for low η the loss is only about a factor 2 more. But in the weak coupling regime the energy loss is significantly more, the energy loss is even several orders of magnitude more. The effects of non-linear coupling have been assumed to converge to the linear model, but it diverges. Until now only simulations with a limiting energy resolution of $\frac{\Delta E}{E_0} \approx 0.01$ were done. This makes it difficult to compare with literature since that regime is not reached in the simulations. But by comparing the fit in the high energy loss regime with literature, it seems that

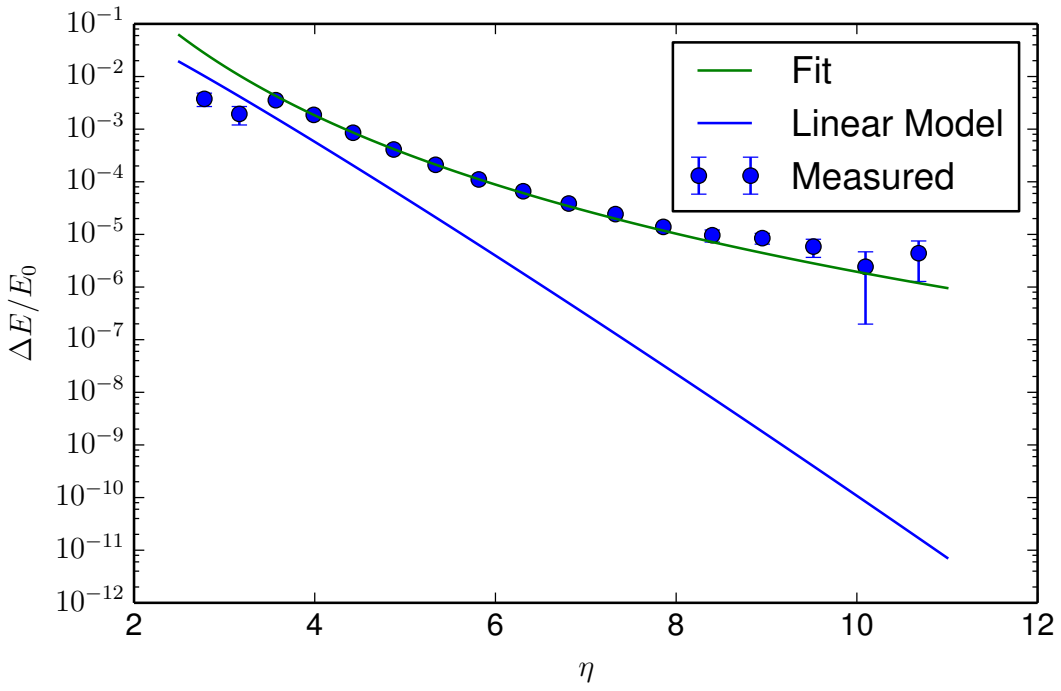

FIGURE 4.1: The energy lost during a tidal interaction against η. Each blue dot is the average of 5 simulations with the same η but different b and v_∞. The error on each measurement is the standard deviation of those 5 simulation. The green line is a fit with a power law and the blue line is the linear model.

results are similar as to what others find. The power law fit has about the same slope as the linear model for $2.0 \leq \eta \leq 3.0$ and the energy loss is about twice as much as predicted, which was also noted by Faber et al. [13]. The power law is chosen as

$$\frac{\Delta E}{E_0} = \alpha \eta^\beta \tag{4.1}$$

By using the linear least square method the fitting parameters are found to be $\alpha = 57.3$ and $\beta = -7.5$. Even though the fit formula is quite simple compared to the linear perturbation theory it performs good. The reduced χ^2 residual is 5.1. Making this a reasonable fit for such a simple model. Mass loss is not included in the linear theory so the first 2 points are not taken into account in the fitting procedure because there mass loss starts to occur see Figure 4.2. An interesting effect is that the energy loss seems to decrease when mass loss occurs. This means that while the star loses orbital energy due to tidal dissipation it also regains some by ejecting mass. A nice idea would be to look if this effect can be used to go from a bound system to a unbound system and perform a tidal release, Faber et al. [13] suggest that it can happen.

To check where the non-linear effects come from, the star is projected on spherical harmonics. According to the theory the dominant spherical harmonics would be the

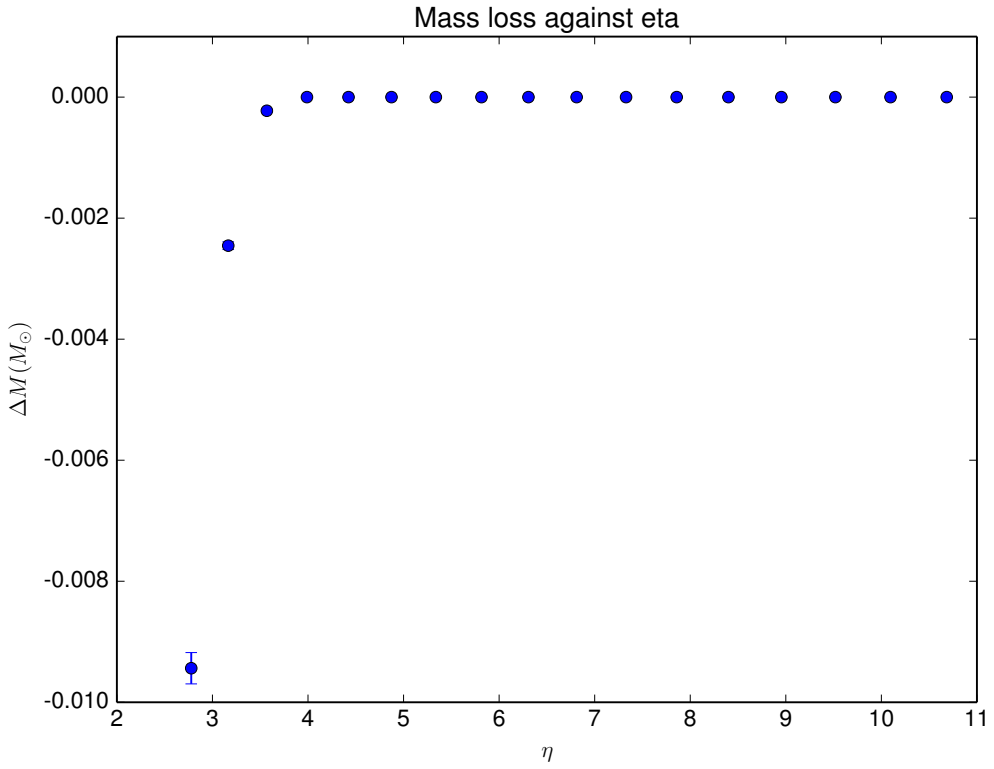

FIGURE 4.2: The mass loss during a tidal encounter. The star loses a low percentage of its mass $\Delta m < 1\%$. It starts to occur at $\eta \leq 3.5$

$l = 2, m = \pm 2$ and the $l = 2, m = 0$ modes. To determine whether that is true the modes up till $l = 4$ are included in the decomposition which can be seen in Figure 4.3. The spherical harmonics that are used are the real spherical harmonics. Two runs are analysed, a run with mass loss and a run without mass loss. The run without mass loss only experiences excitation of the predicted modes, they are several orders of magnitude stronger than other excited modes. In the run with mass loss there is another mode which gets excited and the mode also does not damp out. Snapshots are plotted for a visual check what happens.

In Figure 4.4 a series of snapshots is taken of the same run as in the left plot of Figure 4.3. In the snapshots it is seen that the has a rotating bulge which corresponds with the $l = 2, m = \pm 2$ modes. The right plot of Figure 4.3 is shown in Figure 4.5 which loses mass, the mass loss manifest itself in elongated arms. The dipole moment $l = 1, m = \pm 1$ reacts heavily on this shape. So the appearance of that mode corresponds to the generation of arms where mass loss occurs. The mass is certainly a non-linear effect but for the case of small interaction where no mass loss occurs there is no reason for the non-linear effects. Since only the modes are excited which where predicted by the linear theory. According to Khokhlov et al. [15, 16] the non-linear effects are not

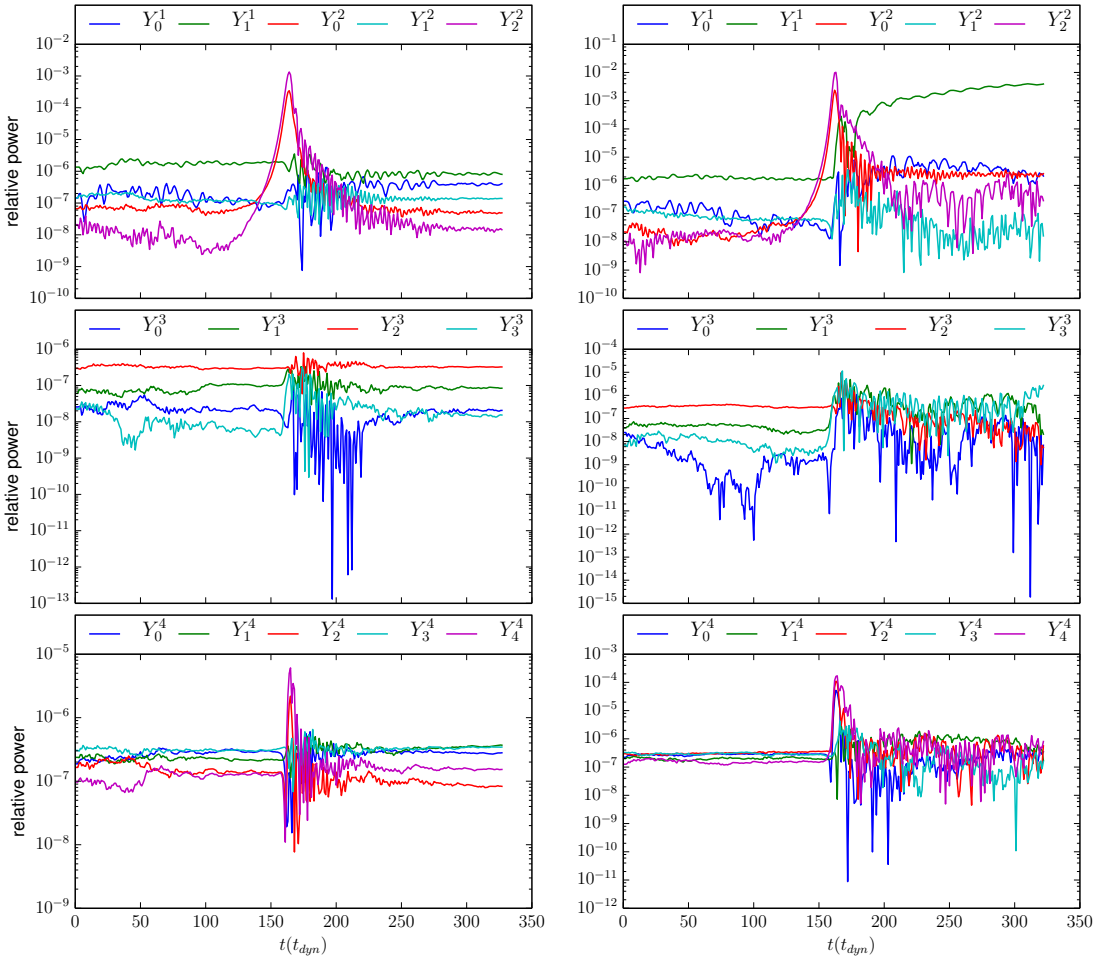

FIGURE 4.3: The relative power with respect tot the Y_0^0 mode of the spherical harmonics. The power is the absolute squared value of the coefficients of the spherical harmonic decomposition. The $\pm m$ modes are summed together since those modes are the same but with a different orientation which is of no interest. Only the power in the modes is needed. The plots on the left side are a run with $\eta = 5.3$ and the plots on the right side have $\eta = 3.6$.

in the non-radial adiabatic oscillations but in the radial oscillations. But due to time constrains this was not looked into.

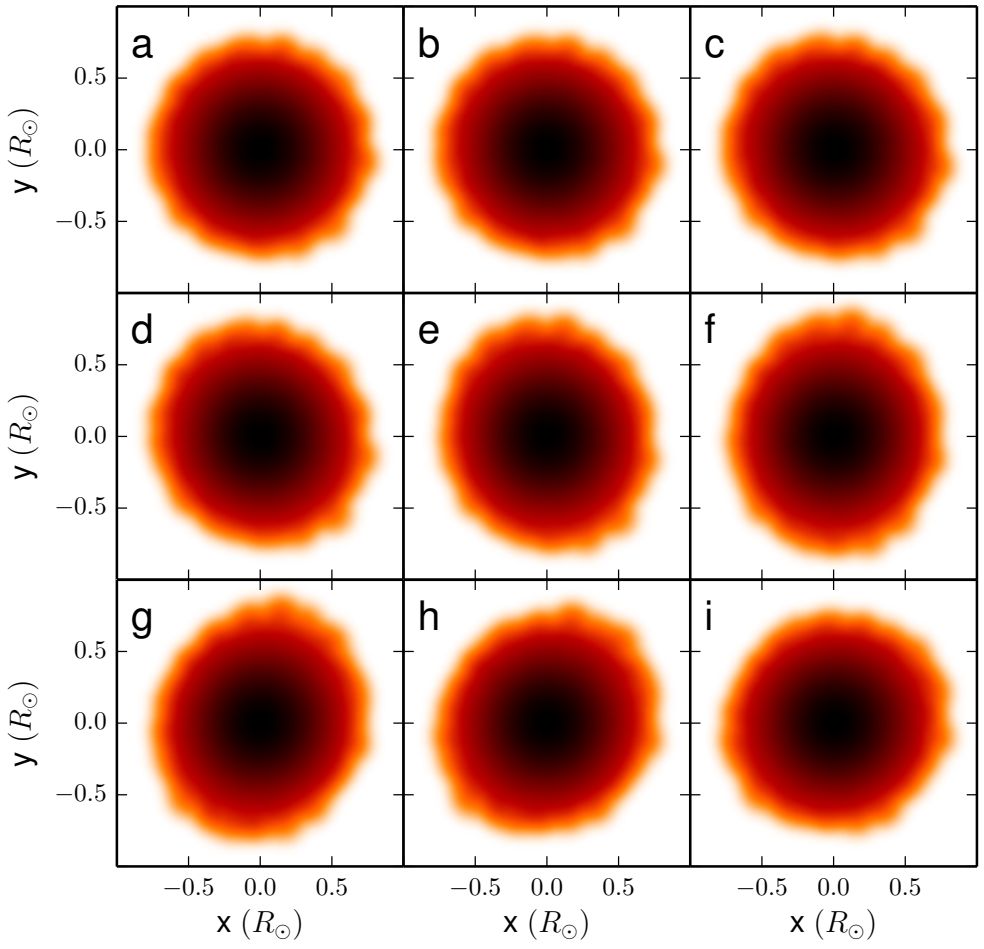

FIGURE 4.4: Snapshots of a run with $\eta = 5.3$. The column density is plotted as seen from a line perpendicular to the orbit plane. Dark is high density and light is low density. This run is in the weak coupling regime. From this figure it can be clearly seen that the dominant modes are the $l = 2, m = \pm 2$.

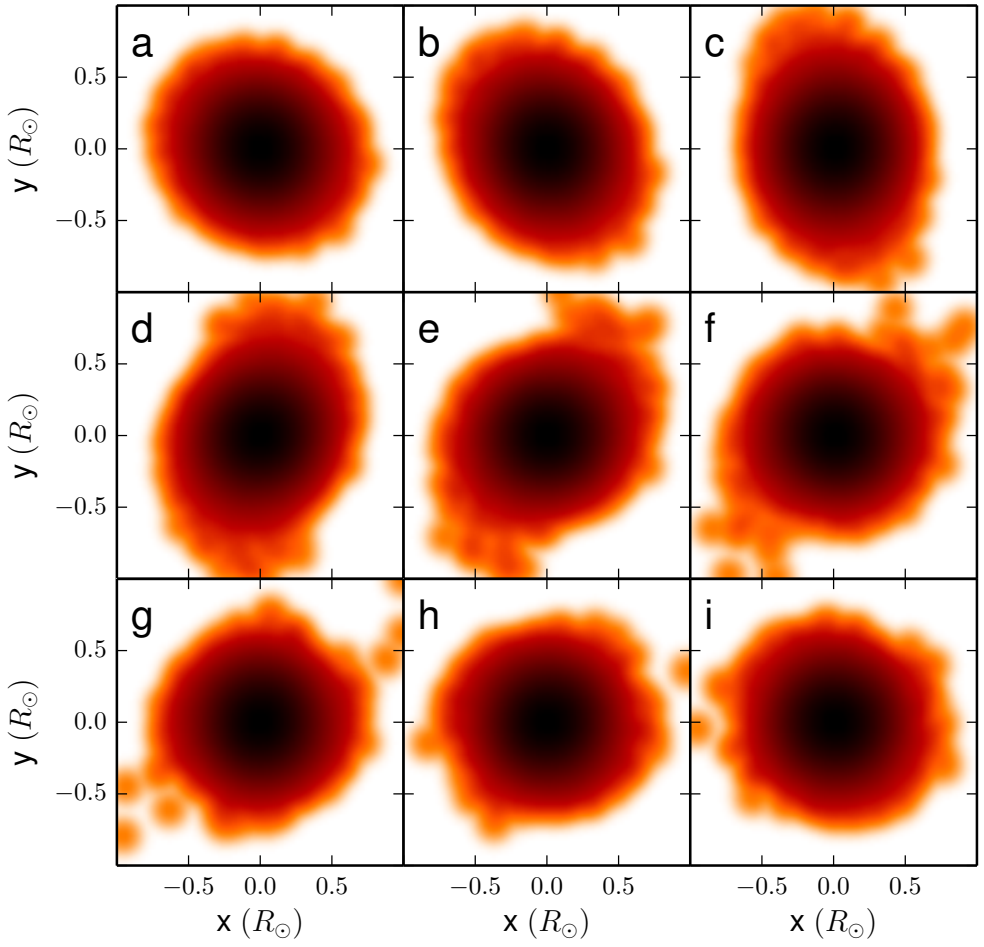

FIGURE 4.5: Snapshots of a run with $\eta = 3.6$. The column density is plotted as seen from a line perpendicular to the orbit plane. Dark is high density and light is low density. This run is in the intermediate coupling regime. This can be seen from the clumps which try to come lose from the bulk in shot g and h. From this figure it can be clearly seen that the dominant modes are the $l = 2, m = \pm 2$ which is the rotating tidal bulge.

Chapter 5

Discussion

5.1 Tidal cross section

These results can now be used to determine a cross section for tidal capture. If the star loses an amount of ΔE during a close passage, the maximum speed it can have in infinity is

$$v = \sqrt{\frac{2\Delta E}{M}} \tag{5.1}$$

If the speed is higher than this the star will not be captured. Using the fit that was found the energy loss can be related to the tidal interaction parameter. Which can then be again related to the impact parameter. The energy loss relation is

$$\alpha\eta^{\beta}\frac{GM^2}{R} = \Delta E \tag{5.2}$$

so combining this with the previous equation leads to

$$\frac{1}{2}Mv_{\infty}^2 = \Delta E = \alpha\eta^{\beta}\frac{GM^2}{R} \tag{5.3}$$

$$\eta = \sqrt[\beta]{\frac{R}{2\alpha GM}v_{\infty}^2} \tag{5.4}$$

This result is then rewritten in the form of the pericenter distance with equation 2.11.

$$r_{min} = \left(\left(\frac{M+M_{bh}}{M}\right)^{\frac{1}{2}}\eta\right)^{\frac{2}{3}}R \tag{5.5}$$

The necessary impact parameter is then found using this pericenter distance and substituting it in equation 2.5. Now η is only a parameter of the speed in infinity, and so are the pericenter distance and the impact parameter. The impact parameter can then

be used to calculate the cross section as

$$\sigma = \pi b^2 \tag{5.6}$$

If all equations are substituted correctly the resulting equation for the cross section will be

$$\sigma = \pi \left(\frac{Rv_\infty^2}{2\alpha GM}\right)^{\frac{4}{3\beta}} \left(\frac{M+M_{bh}}{M}\right)^{\frac{2}{3}} R^2 + \pi \frac{2GM}{v_\infty^2} \left(\frac{Rv_\infty^2}{2\alpha GM}\right)^{\frac{2}{3\beta}} \left(\frac{M+M_{bh}}{M}\right)^{\frac{1}{3}} R \tag{5.7}$$

with α and β the fit parameters. This cross section is larger than the one presented by Press and Teukolsky [5]. They neglect the first term when it should not be neglected. If purely the velocity dependence of the terms is considered the first term grows as $v_\infty^{\frac{8}{3\beta}}$ and the second grows as $v_\infty^{\frac{4}{3\beta}-2}$. If the value for β is filled in the growth rates become $v_\infty^{-0.36}$ and $v_\infty^{-2.18}$. For the larger tidal cross sections the first term is the most important and that is the one that is neglected. So the tidal capture rate is much larger than initially calculated not only because the effect is stronger than what linear theory predicts but also because a part of the cross section was neglected.

The rate of tidal captures is

$$\Gamma = \nu \langle \sigma v \rangle \tag{5.8}$$

here ν is the number density per pc^2 and the bracket means the expectation value weighted by a velocity distribution. If for simplicity an isothermal sphere is assumed this velocity distribution is the Maxwell-Boltzmann distribution which is given as

$$ndv^3 = \frac{4\pi v^2}{\sqrt{(2\pi\Delta v^2)^3}} \exp\left(\frac{-v^2}{2\Delta v^2}\right) dv \tag{5.9}$$

where Δv is the velocity dispersion and v the velocity. The cluster in which HLX-1 is embedded has 2 possible states: a young stellar population or an older stellar population [28]. Farrell et al. [28] argue that the young population is more likely. So for calculation this is also assumed and the relevant numbers are taken from Farrell et al. [28]. For the young population $\nu \approx 120$ pc^{-3} and typical velocity dispersions are $\Delta v \approx 10$ km/s. This gives a rate of $\Gamma = 0.0045$ Myr$^-1$. This is not a high rate if the tidal collision timescale $\Gamma^{-1} = 222$ Myr is compared with the age of the cluster which is around 10-20 Myr. But if there are more young open clusters with intermediate mass black holes, tidal capture would be a reasonable mechanism to explain binary companions. A tidally captured companion would be more likely if the stellar population is older. If the parameters for the older populations from Farrell et al. [28] are used, the number density is then $\nu = 180$ pc^{-3} also with a velocity dispersion of 10 km/s. If these numbers are plugged in the tidal collision timescale would be around the 150 Myr which is shorter than the

proposed age of 200 Myr if the stellar population was old. This tidal capture rate is heavily dependent on the velocity dispersion and that is not known at this moment so the current rates are just estimates. But given these estimates it could be possible to explain the origin of the companion around HLX-1 with a tidal capture.

5.2 Simulation Spikes

There is one main issue with the current simulation setup which can be seen in Figure 5.1. These jumps appear randomly and the cause is not known. This messes up the energy conservation of the orbits. The jumps are in the internal energy and not in the orbital energy which is used to calculate the lost energy. From Figure 4.1 it looks like the jumps do not effect the orbital energy since the standard deviations are very small and the measure points are quite smooth. The jumps occur more often if more time steps are taken or if the amount of particles is increased. It could be that in Gadget there is a bug in the force calculation which occurs when the opening angle is very small. This is something that should be fixed in future work to make the results more reliable.

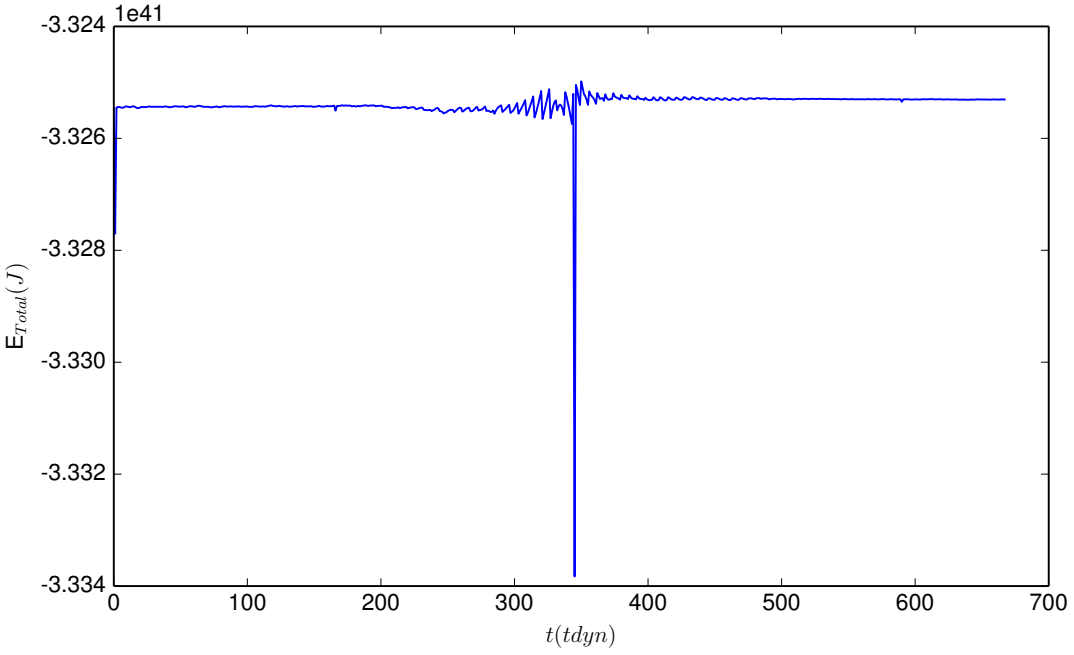

FIGURE 5.1: The evolution of the total energy during a hyperbolic orbit. There are 2 jumps in the energy. One at the beginning and one just past the pericenter.

Chapter 6

Conclusion

6.1 Conclusion

The energy loss during tidal interactions of weak encounters has been under-estimation by order of magnitude in previous works. Using the results from this work tidal capture is possible mechanism to explain companion stars around intermediate mass black holes in open clusters. Several things can still be improved to extend the current simulation code for other problems. The solution for the energy jump problem, which maybe could be solved by replacing the tree code in Gadget by a direct sum method. This would also speed up the current calculations because the tree generation can be skipped. Another extra upgrade would be a set of new smoothing kernels which were introduced last year and these are also explained in [20]. These new SPH kernels would be a better choice for this problem since they are made for compact objects while the current kernels in Gadget are not. This could then also directly be applied to an interesting problem of tidal release. Is it possible to make a bound object go unbound by stripping away its mass? So there are still many possible ways to continue this research.

I would like to thank Nathan de Vries for his help with AMUSE and Gadget. Simon Portegies Zwart for providing this interesting problem and the helpful remarks.

Bibliography

[1] S. A. Farrell, N. A. Webb, D. Barret, O. Godet, and J. M. Rodrigues. An intermediate-mass black hole of over 500 solar masses in the galaxy ESO243-49. *Nature*, 460:73–75, July 2009. doi: 10.1038/nature08083.

[2] C. Hopman, S. F. Portegies Zwart, and T. Alexander. Ultraluminous X-Ray Sources as Intermediate-Mass Black Holes Fed by Tidally Captured Stars. *Astrophysical Journal, Letters*, 604:L101–L104, April 2004. doi: 10.1086/383616.

[3] A. C. Fabian, J. E. Pringle, and M. J. Rees. Tidal capture formation of binary systems and X-ray sources in globular clusters. *Monthly Notices of the RAS*, 172: 15P, August 1975.

[4] H. Baumgardt, C. Hopman, S. Portegies Zwart, and J. Makino. Tidal capture of stars by intermediate-mass black holes. *Monthly Notices of the RAS*, 372:467–478, October 2006. doi: 10.1111/j.1365-2966.2006.10885.x.

[5] W. H. Press and S. A. Teukolsky. On formation of close binaries by two-body tidal capture. *Astrophysical Journal*, 213:183–192, April 1977. doi: 10.1086/155143.

[6] A. G. Kosovichev and A. B. Severnyi. Stellar Oscillations Triggered by Close Encounters. *Soviet Astronomy Letters*, 9:223–227, April 1983.

[7] H. M. Lee and J. P. Ostriker. Cross sections for tidal capture binary formation and stellar merger. *Astrophysical Journal*, 310:176–188, November 1986. doi: 10.1086/164674.

[8] B. Carter and J.-P. Luminet. Tidal compression of a star by a large black hole. I Mechanical evolution and nuclear energy release by proton capture. *Astronomy and Astrophysics*, 121:97–113, May 1983.

[9] B. Carter and J. P. Luminet. Mechanics of the affine star model. *Monthly Notices of the RAS*, 212:23–55, January 1985.

[10] A. Nduka. The Roche Problem in an Eccentric Orbit. *Astrophysical Journal*, 170: 131, November 1971. doi: 10.1086/151194.

[11] A. G. Kosovichev and I. D. Novikov. Non-linear effects at tidal capture of stars by a massive black hole. I - Incompressible affine model. *Monthly Notices of the RAS*, 258:715–724, October 1992.

[12] P. Diener, A. G. Kosovichev, E. V. Kotok, I. D. Novikov, and C. J. Pethick. Non-linear effects at tidal capture of stars by a massive black hole - II. Compressible affine models and tidal interaction after capture. *Monthly Notices of the RAS*, 275: 498–506, July 1995.

[13] J. A. Faber, F. A. Rasio, and B. Willems. Tidal interactions and disruptions of giant planets on highly eccentric orbits. *Icarus*, 175:248–262, May 2005. doi: 10.1016/j.icarus.2004.10.021.

[14] S. Yamada, A. T. Okazaki, and M. Y. Fujimoto. Tidal Interactions of Red Giants with Environment Stars in Globular Clusters. *Astrophysical Journal*, 678:922–938, May 2008. doi: 10.1086/533516.

[15] A. Khokhlov, I. D. Novikov, and C. J. Pethick. Weak Tidal Encounters of a Star with a Massive Black Hole. *Astrophysical Journal*, 418:163, November 1993. doi: 10.1086/173379.

[16] A. Khokhlov, I. D. Novikov, and C. J. Pethick. Strong Effects during Close Encounters of a Star with a Massive Black Hole. *Astrophysical Journal*, 418:181, November 1993. doi: 10.1086/173380.

[17] F. I. Pelupessy, A. van Elteren, N. de Vries, S. L. W. McMillan, N. Drost, and S. F. Portegies Zwart. The Astrophysical Multipurpose Software Environment. *Astronomy and Astrophysics*, 557:A84, September 2013. doi: 10.1051/0004-6361/201321252.

[18] G. L. Cassiday G. R. Fowles. 6. gravitation and central forces. In *Analytical Mechanics*. Cengage Learning, Inc., 2007.

[19] R. A. Gingold and J. J. Monaghan. Smoothed particle hydrodynamics - Theory and application to non-spherical stars. *Monthly Notices of the RAS*, 181:375–389, November 1977.

[20] S. Rosswog. SPH Methods in the Modelling of Compact Objects. *ArXiv e-prints*, June 2014.

[21] P. P. Eggleton. The evolution of low mass stars. *Monthly Notices of the RAS*, 151: 351, 1971.

[22] E. Glebbeek, O. R. Pols, and J. R. Hurley. Evolution of stellar collision products in open clusters. I. Blue stragglers in N-body models of M 67. *Astronomy and Astrophysics*, 488:1007–1015, September 2008. doi: 10.1051/0004-6361:200809930.

[23] V. Springel. The cosmological simulation code GADGET-2. *Monthly Notices of the RAS*, 364:1105–1134, December 2005. doi: 10.1111/j.1365-2966.2005.09655.x.

[24] F.I. Pelupessy. *Numerical studies of the interstellar medium on galactic scales*. PhD thesis, Leiden Observatory, 2005.

[25] F. I. Pelupessy, J. Jänes, and S. Portegies Zwart. N-body integrators with individual time steps from Hierarchical splitting. *New Astronomy*, 17:711–719, November 2012. doi: 10.1016/j.newast.2012.05.009.

[26] P. Hut, J. Makino, and S. McMillan. Building a better leapfrog. *Astrophysical Journal, Letters*, 443:L93–L96, April 1995. doi: 10.1086/187844.

[27] S. F. Portegies Zwart and A. T. Meinen. Quick method for calculating energy dissipation in tidal interaction. *Astronomy and Astrophysics*, 280:174–176, December 1993.

[28] S. A. Farrell, M. Servillat, J. Pforr, T. J. Maccarone, C. Knigge, O. Godet, C. Maraston, N. A. Webb, D. Barret, A. J. Gosling, R. Belmont, and K. Wiersema. A Young Massive Stellar Population around the Intermediate-mass Black Hole ESO 243-49 HLX-1. *Astrophysical Journal, Letters*, 747:L13, March 2012. doi: 10.1088/2041-8205/747/1/L13.